

Article

https://doi.org/10.1038/s41560-025-01714-y

Direct air capture of CO₂ for solar fuel production in flow

Received: 27 February 2024

Accepted: 10 January 2025

Published online: 13 February 2025



Sayan Kar ®, Dongseok Kim, Ariffin Bin Mohamad Annuar ®, Bidyut Bikash Sarma ®, Michael Stanton, Erwin Lam, Subhajit Bhattacharjee, Suvendu Karak, Heather F. Greer & Erwin Reisner ® ⊠

Direct air capture is an emerging technology to decrease atmospheric CO₂ levels, but it is currently costly and the long-term consequences of CO₂ storage are uncertain. An alternative approach is to utilize atmospheric CO₂ on-site to produce value-added renewable fuels, but current CO₂ utilization technologies predominantly require a concentrated CO₂ feed or high temperature. Here we report a gas-phase dual-bed direct air carbon capture and utilization flow reactor that produces syngas (CO + H₂) through on-site utilization of air-captured CO₂ using light without requiring high temperature or pressure. The reactor consists of a bed of solid silica-amine adsorbent to capture aerobic CO₂ and produce CO₂-free air; concentrated light is used to release the captured CO₂ and convert it to syngas over a bed of a silica/alumina-titania-cobalt bis(terpyridine) molecular-semiconductor photocatalyst. We use the oxidation of depolymerized poly(ethylene terephthalate) plastics as the counter-reaction. We envision this technology to operate in a diurnal fashion where CO₂ is captured during night-time and converted to syngas under concentrated sunlight during the day.

Direct air capture (DAC) of carbon dioxide (CO₂) is a promising technology for actively removing CO_2 from the atmosphere and combating the climate crisis^{1,2}. Despite the advancements and pilot-scale implementations, DAC remains an energy-intensive process, leading to high costs for CO₂ removal while not producing any products of economic value^{3,4}. This limitation confines the technology to localized environments with inexpensive energy sources. Some state-of-the-art DAC technologies operate by carbon capture and storage, where the captured CO₂ is stored under geological formations⁵. However, the long-term effects of storing vast amounts of CO₂ underground over decades remain uncertain⁶. An alternative is to utilize the captured CO₂ to produce renewable fuels and chemicals, thereby creating value while achieving a carbon-neutral cycle^{7,8}. Nevertheless, most prominent CO₂ utilization (CO_2U) technologies require pure CO_2 as the carbon feed while needing high energy input by themselves, making their overall integration in the DAC framework challenging.

Solar-powered technologies offer a sustainable future where we can harness the Sun's energy directly to fuel our economy $^{9\text{-}11}$. Solar-driven CO2-to-fuel synthesis has been explored extensively in

recent decades, primarily in solid-liquid interfaces 12-14. Solution-based systems often face limitations due to the low solubility of CO₂ in the aqueous medium. To circumvent this, gas-phase CO₂ photoreduction processes are emerging, which offer enhanced local CO₂ concentration, better mass transport and reduced light scattering, among other advantages¹⁵⁻¹⁹. Despite the benefits, gas-phase reports mostly show limited activities due to the challenging thermodynamics of gas-phase CO₂ reduction^{20,21}. The processes are further limited by the requirement of pure CO₂ (whose production from emission sources is cost-intensive with US\$125-335 per ton of CO₂ from the air²²) and are often sensitive to oxygen in the feed stream. From a materials perspective, gas-phase CO₂ photoreduction catalysts typically use metal/metal oxide composites that require high overpotentials, resulting in low efficiency and selectivity. In this context, the use of molecular-semiconductor hybrid materials represents an underexplored approach for combining a molecular catalyst's high activity and selectivity with the durability and robustness of heterogeneous solid support^{23,24}.

Here, we report an integrated gas-phase direct air carbon capture and utilization (DACCU) flow reactor that captures CO_2 from air,

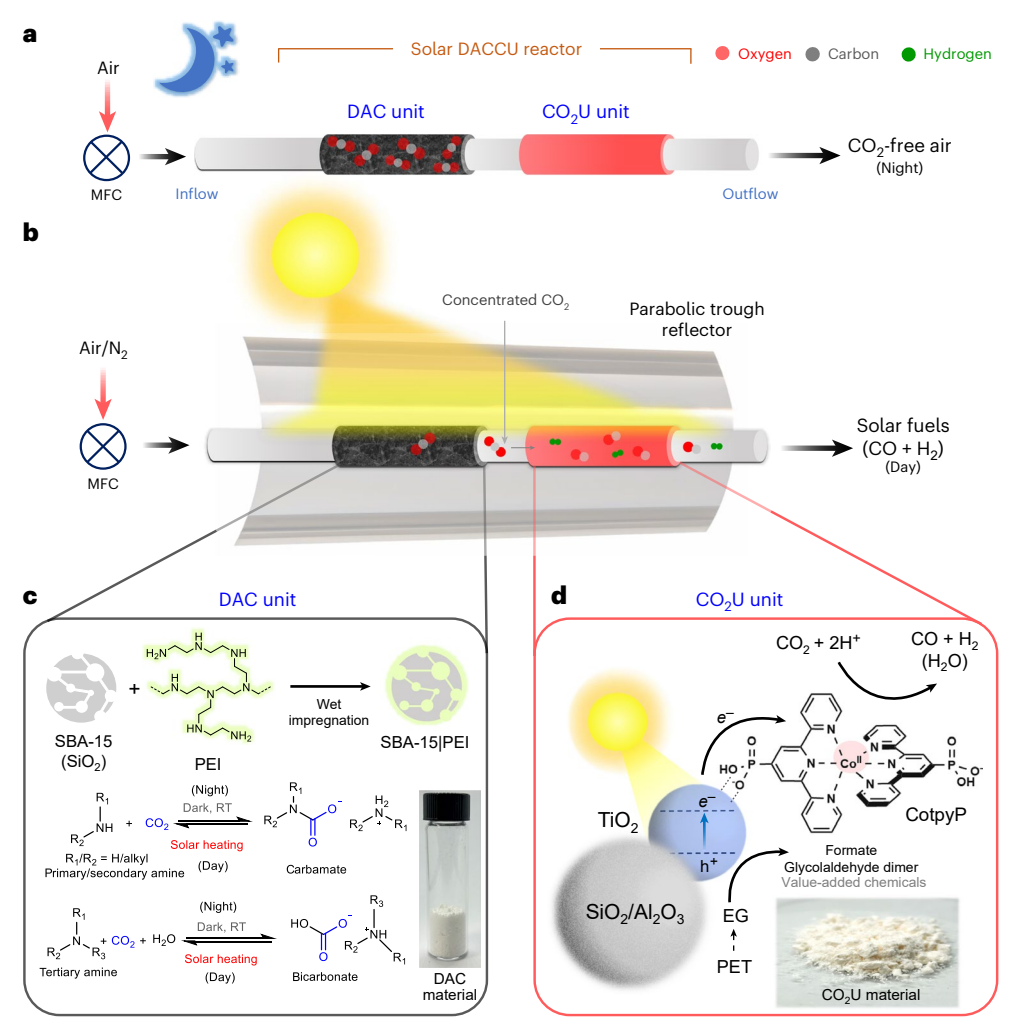


Fig. 1 | DACCU through a dual-bed flow reactor consisting of DAC and CO_2U units. a, Schematics of the system during light-off night operation. b, Schematics of the overall system during light-on day operation. c, The carbon capture unit with chemical CO_2 capture and release equations. d, The solar-driven CO_2U unit

material composition and the relevant reduction and oxidation reactions. RT, room temperature; MFC, mass flow controller; PEI, polyethyleneimine; PET, poly(ethylene terephthalate); EG, ethylene glycol.

concentrates it and converts it into renewable fuel using simulated sunlight (Fig. 1a.b). The dual-bed reactor can be envisioned to operate in a diurnal cycle, where CO₂ is chemically captured from the air during light-off (night-time) operation while letting the other gases (for example, N₂ and O₂) pass through. The captured CO₂ is released in a concentrated stream during the light-on (daytime) operation and further photochemically converted into synthesis gas (in short, syngas, a mixture of CO and H₂ that is used as a precursor for fuel and chemical synthesis). DAC is enabled by a state-of-the-art solid-phase silica-polyamine CO₂ adsorber that desorbs the captured CO₂ at elevated temperatures (80-100 °C) provided by photothermal solar heating (Fig. 1c)^{25,26}. We use a parabolic trough solar collector that concentrates (simulated) sunlight to heat the adsorbent for efficient CO₂ release while enhancing photoconversion of released CO₂. Light-driven CO₂-to-fuel synthesis is enabled by a developed alumina/ silica-titania-cobalt bis(terpyridine) (Al₂O₃/SiO₂|TiO₂|CotpyP) hybrid material that is efficient in gas-phase CO₂U in a moist fixed-bed flow reactor setup (Fig. 1d). Poly(ethylene terephthalate) (PET)-derived ethylene glycol (EG) is used as the reductant. This work demonstrates the ability of a molecular-semiconductor hybrid to catalyse gas-phase CO₂ photoreduction while offering a solution to manage atmospheric O₂ in aerobic CO₂ photoreduction via temporal separation between CO₂ capture and conversion.

DAC and photothermal CO₂ release

The first step towards assembling the envisioned integrated solar-powered DACCU flow reactor was developing a solar DAC unit to capture and concentrate aerobic CO₂ that would act as the carbon source to a downstream CO₂U unit (Fig. 1a,b). For this purpose, branched polyethyleneimine (PEI, weight-average molecular weight 25,000 g per mole) was impregnated as an active CO₂-capturing chemical onto a porous solid support of mesoporous silica (SBA-15, particle size <150 μm) in equal weight by wet impregnation to obtain a solid CO₂ adsorbent powder (SBA-15|PEI). Thermogravimetric analysis (TGA) of the adsorbent in air showed 50 wt% PEI loading onto the silica support (Supplementary Fig. 1a). Effective deposition of the amine throughout silica pores was verified by Brunauer-Emmett-Teller (BET) isotherm analysis, which showed a reduced surface area upon PEI incorporation onto the support (9.2 m² g⁻¹ versus 300 m² g⁻¹ for the parent silica support; Supplementary Fig. 1b). Uniform deposition of PEI on silica was also observed by scanning electron microscopy (SEM)-energy-dispersive X-ray spectroscopy (EDS) mapping of the adsorbent (Supplementary Figs. 2 and 3). Similar CO₂ scrubbers with optimal amounts of polyamines deposited over solid supports (Supplementary Note 1) are well established in the literature for DAC and have applications in state-of-the-art CO₂ removal technologies owing to their efficient CO₂ capture kinetics and fast CO₂ release at elevated temperatures^{27,28}.

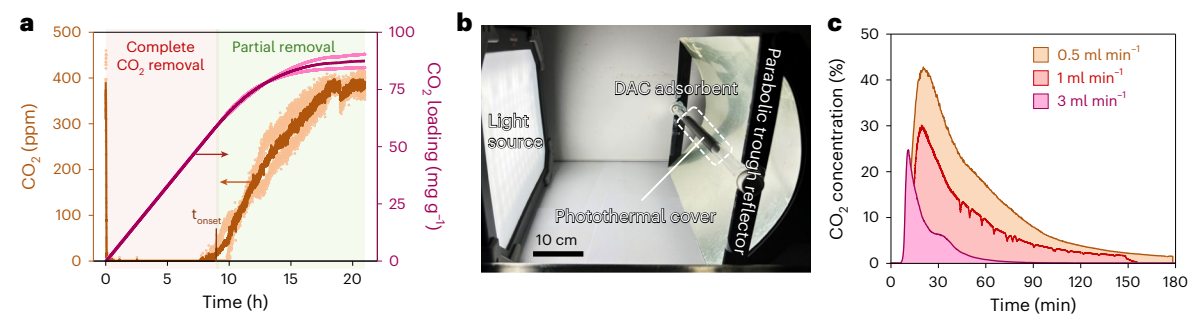


Fig. 2 | **DAC** and solar-driven photothermal release of CO_2 , a, CO_2 levels in the outflow during DAC and the adsorbed CO_2 amount over time. DAC was performed with 600 mg of SBA-15|PEI adsorbent with an airflow rate of 90 ml min⁻¹ at room temperature. **b**, Photothermal CO_2 desorption setup with photothermal coating and parabolic trough reflector (note that the light source is for demonstration purposes only and different from the actual solar simulator

used). **c**, CO₂ concentration in outflow gas stream during release with different flow rates under 3 suns of solar irradiation with photothermal cover. In all cases, the adsorbent bed temperatures reached around 85–100 °C across different regions under concentrated light during desorption. For **a**, data are presented as the average of two independent runs and the individual data points are shown in hollow circles.

DAC experiments with the synthesized solid CO2 adsorber (SBA-15|PEI) were carried out with a fixed bed of SBA-15|PEI (600 mg, length 5 cm) inside a glass tube reactor (inner diameter 0.6 cm) by flowing humidified air (400 ppm CO_2 in 21% O_2 and balance N_2) through it at ambient temperature (flow rate 90 ml min⁻¹; Supplementary Fig. 4a). Analysis of the CO₂ concentration in the outflow showed complete CO₂ removal for around 9 h of operation (Fig. 2a), followed by a slow increase in CO₂ level consistent with the onset of saturation of the capture material. Complete CO₂ saturation was reached after 18 h, at which time the total CO₂ intake of the composite by DAC was estimated around $87 \pm 4 \,\text{mg}$ of CO_2 per gram of adsorbent (0.17 \pm 0.01 mol of CO_2 per mole of amine) as determined from the CO₂ concentration-time curve integral (Fig. 2a). The observed timescale for capture (10-16 h) is optimal for night-time operation and complements the average daily sunlight exposure of many tropical and subtropical regions. Furthermore, the complete capture duration (t_{onset}) is proportional to the mass of the adsorbent and inversely proportional to the flow rate and, thus, can be tuned by changing these two parameters accordingly.

Solar-driven photothermal release of CO₂ from the adsorbent was then explored by irradiating the post-capture adsorber bed with simulated sunlight (1 sun, 100 mW cm⁻², AM 1.5G) under airflow (1 ml min⁻¹) at ambient pressure. Under these standardized conditions, no CO₂ release in the outflow was detected. Thermal image analysis of the system showed a temperature of 35 °C at the adsorber bed upon light irradiation, which is insufficient for the thermal desorption of the captured CO₂ (refs. 25,26). However, increasing the reactor bed temperature via a combination of concentrating light using a parabolic trough reflector (to 3 suns) and covering the outside of the adsorber bed with an infrared (IR) absorbing photothermal black tape (Methods) resulted in efficient CO₂ release (Fig. 2b,c and Supplementary Figs. 4 and 5). Under these conditions, the temperature of the adsorbent reached around 100 °C at 1 ml min⁻¹ flow rate (Supplementary Fig. 6), while the CO₂ concentration in the outflow reached 30% (v/v) within 30 min of solar irradiation (Fig. 2c). The CO_2 levels in the outflow from solar-driven photothermal desorption decreased below 2% (v/v) after approximately 2 h. Higher CO₂ concentration in the outflow stream (42%) for a longer duration can be obtained by decreasing the flow rate to 0.5 ml min⁻¹, whereas increasing the flow rate of the carrier gas results in a quicker desorption process with lower CO₂ concentrations in the outflow (Fig. 2c; note the decreasing area under the curve with higher flow rate, reflecting similar total CO₂ desorption, calculated as the area × flow rate). The solar-to-CO₂ release energy efficiency of the process is estimated at around 0.6% (Supplementary Note 2). SEM and EDS analysis of the post-capture-release adsorbent showed comparable morphological structures and organic content to the pre-capture material, reflecting minimal changes during the cycle (Supplementary Fig. 7), and the adsorbent can be reused in CO_2 capture for multiple cycles without a notable performance decrease (Supplementary Fig. 8).

Gas-phase CO₂-to-fuel utilization in flow

The development of an efficient, inexpensive moist-bed gas-phase CO₂-to-fuel utilization system was explored next, to be placed downstream to the solar DAC and release unit (Fig. 1b). Most reports on gas-phase CO₂ reduction focus on water oxidation as the counter-reaction, which is kinetically and thermodynamically challenging ($\Delta G \approx +237$ kJ mol⁻¹). Consequently, we replaced water oxidation with a favourable alcohol oxidation reaction ($\Delta G \ll 237 \text{ kJ mol}^{-1}$) to enhance the CO₂ reduction rates²⁹⁻³¹. This imparts additional advantages to the system, including ease of generated syngas post-processing and avoidance of explosive oxygen-fuel gas mixture formation (Supplementary Note 3). The alcohols can be sourced from different waste streams, including depolymerized discarded plastics (EG), biorefineries (glycerol) and biomass (sugars), and can be upgraded in our DACCU process to value-added chemicals^{32–34}. For the solar-driven conversion, TiO₂ (P25) is used as an inexpensive photocatalyst, along with a chemically immobilized cobalt (II)-based molecular catalyst (CotpyP) as the CO₂ reduction co-catalyst to reduce the required overpotential ^{35,36}. For gas-phase operation, we further distributed the TiO₂|CotpyP over a porous high-surface-area solid support (silica or alumina) to facilitate gas transport that enhances the CO₂U rates (Fig. 1d).

The CO₂U material was synthesized by stirring a solution of CotpyP (0.5 mg) and TiO₂ nanoparticles (50 mg, particle size 21 nm) in MeOH (for immobilization of CotpyP via its phosphonic acid linkers on the TiO_2 surface) followed by the addition of SiO_2 nanoparticles ($nSiO_2$, 1g, particle size 5-20 nm) as a high-surface-area support. Solvent removal under vacuum after overnight stirring afforded a beige-coloured solid powder of the hybrid composite (nSiO₂|TiO₂|CotpyP) for CO₂ conversion. Scanning transmission electron microscopy (STEM)-EDS mapping of the composite showed uniform distribution of TiO₂ nanoparticles with amorphous phase SiO₂ throughout (Fig. 3a and Supplementary Fig. 9). Although the loading of molecular cobalt catalyst in the composite was below the detection limit by elemental mapping, uniformly immobilized CotpyP on TiO2 surfaces was indirectly observed by C,N EDS mapping. Inductively coupled plasma optical emission spectroscopy (ICP-OES) analysis confirmed the presence of Co and showed around 0.6 µmol of Coper gram of catalyst loading. The IR and ultraviolet-visible (UV-vis) diffuse reflectance spectra showed characteristic absorption peaks of both TiO₂ and CotpyP molecular complex, using a higher loading to increase signal intensities (Supplementary Fig. 10a,b). BET isotherm revealed a high surface area (494 m² g⁻¹) and

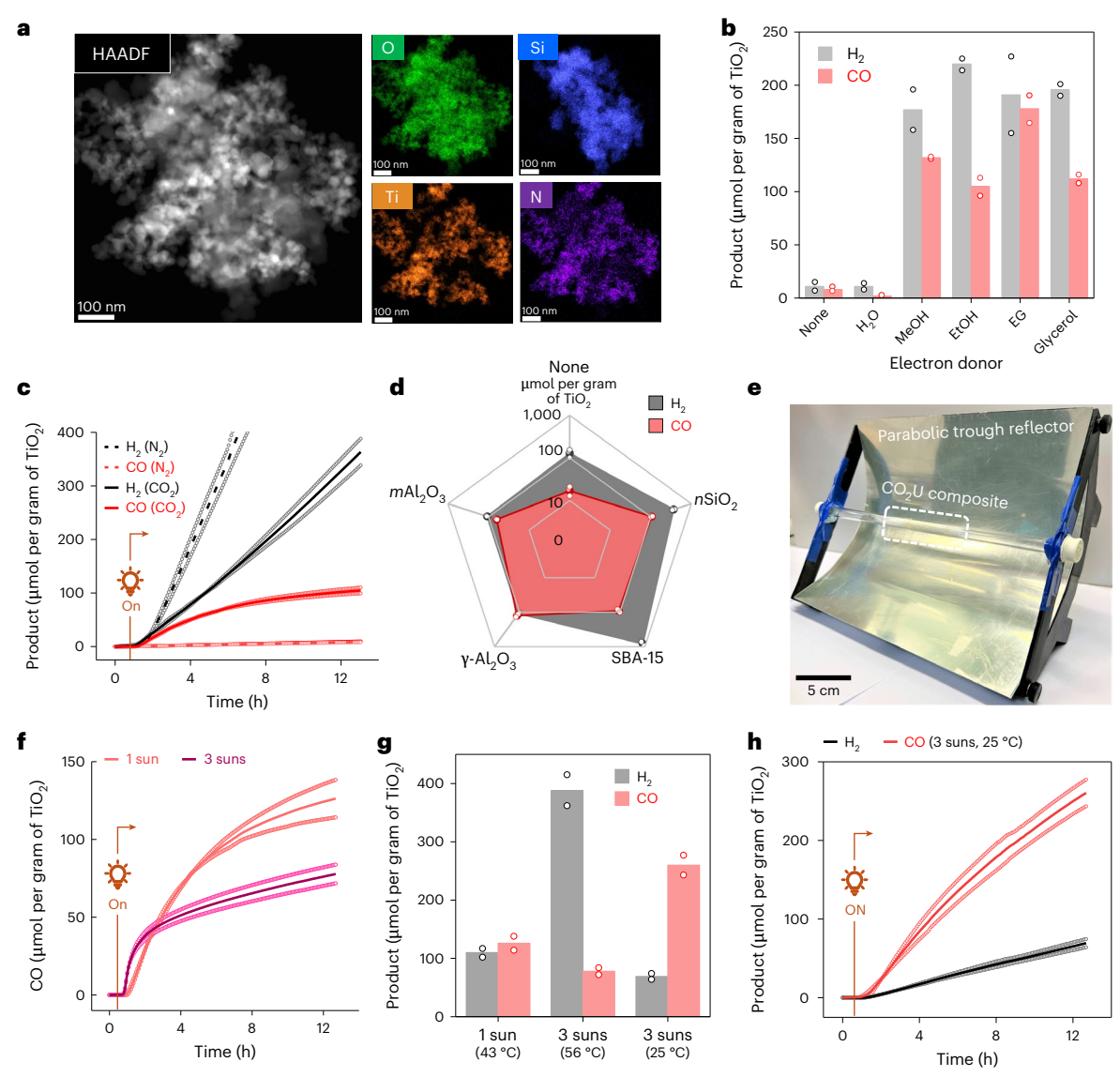


Fig. 3 | **Characterization and performance of the CO_2U unit. a**, HAADF-STEM image and the relevant EDS maps (O, Si, Ti, N) of the composite. **b**, The effect of different alcohol electron donors on H $_2$ and CO formation. Reactions were carried out in batch with 100 mg of CO $_2$ U composite (nSiO $_2$ |TiO $_2$ |CotpyP) and 0.15 ml of electron donor under 1 sun (100 mW cm $^{-2}$, AM1.5G) for 20 h. **c**, The effect of N $_2$ versus CO $_2$ carrier gas on product formation in fixed-bed flow setup. Reactions were performed with 250 mg of CO $_2$ U composite, moistened with 0.50 ml EG, under 1-sun illumination at a carrier gas flow rate of 1 ml min $^{-1}$. **d**, The effect of different support materials on performance under similar conditions. **e**, An image of the parabolic trough reflector used for light concentration with

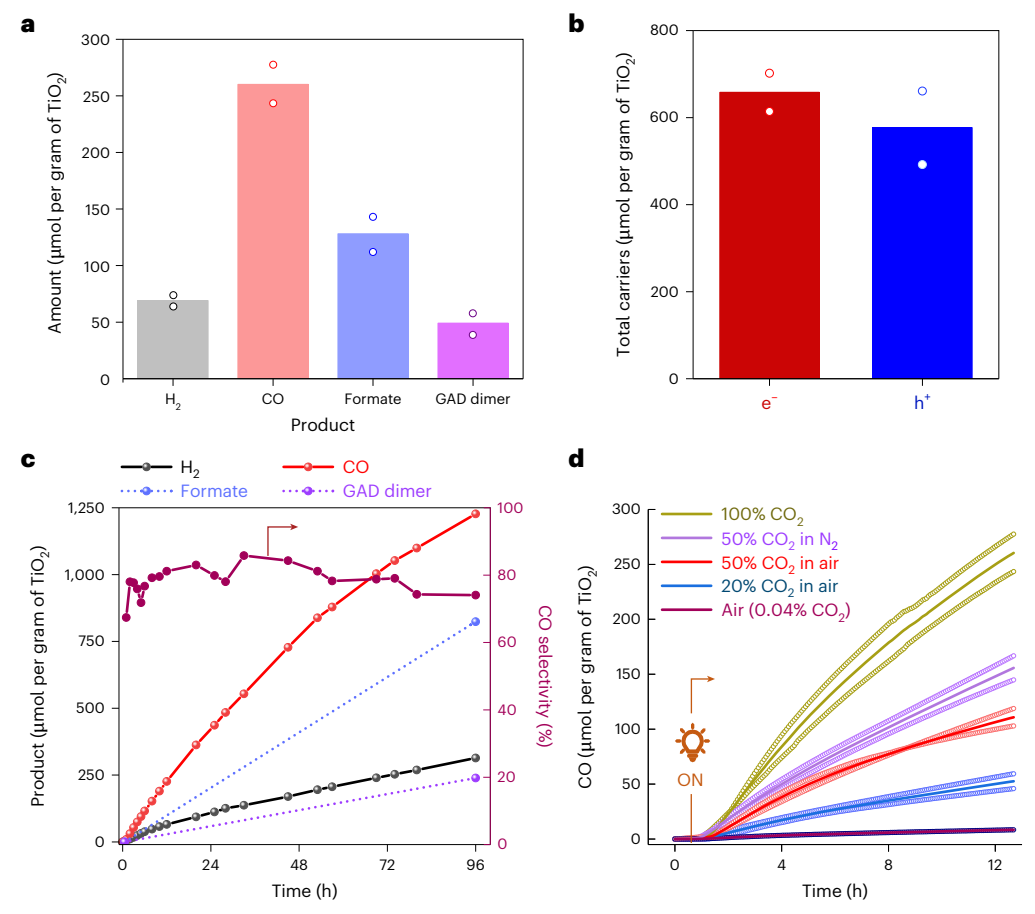
the mounted tubular fixed-bed reactor. **f**, The effect of increasing solar intensity (around 3 suns) via reflector on CO formation when using $\gamma\text{-Al}_2O_3|\text{TiO}_2|\text{CotpyP}$ as the CO $_2\text{U}$ composite. **g**, The effect of temperature regulation on CO and H $_2$ formation. The 43 °C and 56 °C reactions were performed without temperature regulation (elevated temperatures due to solar thermal heating), whereas in the 25 °C reaction, temperature was kept steady using a water jacket. **h**, Product evolution with time under 3-sun illumination when temperature was kept steady at 25 °C. For **b**–**d** and **f**–**h**, data are presented as the average of two independent runs and the individual data points are shown in hollow circles.

pore volume $(0.502 \text{ cm}^3 \text{ g}^{-1})$, suggesting the ease of gas penetration (Supplementary Fig. 11)

The solid composite was then used in solar CO_2 conversion to syngas. Initial batch experiments showed that several alcohols, including methanol, ethanol, EG and glycerol, can act as efficient electron donors in the system for syngas formation by CO_2 photoreduction, consistent with the high photoactivity of TiO_2 towards alcohol oxidation (Fig. 3b) 37,38 . The solid composite (250 mg, containing 12.5 mg TiO_2) was then loaded inside a glass tube (inner diameter 0.6 cm) to prepare a fixed-bed flow photoreactor (bed length $^{-2}$ cm). The bed was manually moistened with EG before experiments, acting as an electron donor. For the experiments, humid CO_2 or N_2 was passed through the tube reactor as the carrier gas at a flow rate of 1 ml min $^{-1}$ (gas residence time in the CO_2 U reactor bed $^{-3}$ 5 s) while keeping the catalytic bed

irradiated under simulated sunlight (1 sun,100 mW cm $^{-2}$, AM1.5G). The outflow gas was analysed by gas chromatography (GC) (Supplementary Fig. 12). Under these conditions, CO and H $_2$ formation were observed in the outflow when CO $_2$ was used as the carrier gas, with respective yields of 105 ± 8 µmol per gram of TiO $_2$ and 363 ± 35 µmol per gram of TiO $_2$ after 12 h (Fig. 3c). These values are comparable to the reported activities of the catalytic system in solution, without the need for any organic solvent or buffer solution, highlighting the advantages of a fixed-bed gas-phase flow setup 35 . These results also showcase the excellent promise of molecular catalysts immobilized onto a semiconductor surface in moist-bed gas-phase CO $_2$ photoreduction.

A control experiment with humid N_2 as a carrier gas showed only H_2 formation (885 ± 41 μ mol per gram of TiO₂) with minor CO generation, reflecting CO₂ reduction to be the source of CO (Fig. 3c). CO₂ as the CO



 $\label{eq:Fig.4} \textbf{Fig. 4} \ | \ \textbf{CO}_2 \textbf{U} \ \textbf{oxidation product analysis and dilute CO}_2 \ \textbf{response. a}, \ \textbf{The overall reduction and oxidation products observed} \ (\gamma \cdot \textbf{Al}_2 \textbf{O}_3 \ | \ \textbf{TiO}_2 \ | \ \textbf{CotpyPas CO}_2 \textbf{U} \ \textbf{composite and EG} \ \textbf{as electron donor, reaction time 12 h). b}, \ \textbf{Total charge carriers} \ \textbf{involved in product formation. c}, \ \textbf{Long-term product formation activities and} \ \textbf{CO selectivity when PET-derived EG} \ \textbf{was used as reductant} \ (\textbf{for the EG} \ \textbf{derivation}) \ \textbf{CO}_2 \ \textbf{Constant product} \ \textbf{CO}_3 \$

protocol from PET, see Methods). Reaction was performed at a CO_2 flow rate of 3 ml min $^{-1}$. **d**, The effect of CO_2 dilution on CO generation in different carrier gases (CO_2 in nitrogen, air). All reactions were performed under 3-sun illumination at 25 °C temperature. For **a**, **b** and **d**, data are presented as the average of two independent runs and the individual data points are shown in hollow circles.

source was further verified by isotopic labelling, where using $^{13}\text{CO}_2$ as the reactant selectively produced ^{13}C -labelled CO as the product (Supplementary Fig. 13). Another control experiment with $n\text{SiO}_2|\text{TiO}_2$ composite without CotpyP yielded only H_2 and minor CO, confirming the role of the molecular catalyst in CO_2 reduction (Supplementary Fig. 14). The major proton source in the system is probably the dissolved moisture in the humid carrier gas, although EG might also act as a minor proton source as suggested by an isotopic labelling study with EG-D $_6$ (Supplementary Fig. 15). STEM–EDS and powder X-ray diffraction analysis of the post-catalysis composite did not show any trace of Co aggregates, suggesting the immobilized CotpyP as the active CO $_2$ U catalyst (Supplementary Figs. 16 and 17).

The support is an important component in the catalytic system that provides a matrix to the cobalt catalytic centres and allows efficient gas transport through the material (Fig. 3d and Supplementary Fig. 18). Reflecting this, a notable decrease in CO formation was observed (-6 times) when $TiO_2|CotpyP$ was used in the catalytic bed without a support matrix (Fig. 3d). The support also influences the composition of the produced syngas by altering the local catalytic environment ³⁹. Thus, H_2 formation increased (by two to three times) when mesoporous silica (SBA-15) was used as support instead of silica nanoparticles (Fig. 3d and Supplementary Fig. 18). By contrast, the use of alumina support suppressed the H_2 formation while enhancing the CO production, probably due to the altered surface chemistry involving aluminium hydroxyl groups of the alumina ⁴⁰. From screening several supports, activated γ -alumina nanoparticles (γ -Al₂O₃, particle size <50 nm) were

found to be the most suitable support material for our system owing to the observed high CO $_2$ reduction rates (126 \pm 17 μmol of CO per gram of TiO $_2$ after 12 h). The resultant syngas was rich in CO (CO:H $_2$ 5:4), ideal for downstream applications ranging from liquid fuel production to chemical syntheses 41 .

The effect of concentrated sunlight on the system was explored with the γ-Al₂O₃|TiO₂|CotpyP composite by placing the tube reactor at the focal axis of a parabolic trough reflector where the light intensity reached up to 300 mW cm⁻² (Fig. 3e). Under concentrated light, high H₂ and CO formation were observed for 0.5 h, followed by a decrease in CO production (Fig. 3f). The decrease is probably due to the increased temperature of the reactor bed under light concentration, reaching 56 °C during the reaction (Supplementary Fig. 19) and causing partial deactivation of the molecular catalyst (Supplementary Fig. 20). To circumvent this, a water jacket was introduced around the CO₂U chamber, and the temperature was kept constant at 25 °C. This resulted in a high and steady CO formation with yields reaching $260 \pm 24 \mu mol per$ gram of TiO₂ after 12 h (Fig. 3g,h). The produced syngas was CO rich because of the suppressed H_2 formation at this temperature (CO: H_2 4:1; Supplementary Fig. 21). The turnover number (TON) of the molecular catalyst CotpyP after this time is calculated as 21 ± 2 with a turnover frequency (TOF) of $1.8 \pm 0.1 \,h^{-1}$ (Supplementary Fig. 22). The TON can be increased further to 96 ± 7 (TOF $8.0 \pm 0.6 \,h^{-1}$) by decreasing the CotpyP loading onto the composite from 0.05 wt% to 0.005 wt%, but this also decreases overall CO formation (116 ± 9 μmol per gram of TiO₂ after 12 h; Supplementary Fig. 22).

High-performance liquid chromatography (HPLC) analysis of an aqueous extract from the post-catalysis reactor bed showed formate and glycolaldehyde (GAD) dimer (molar ratio ~5:2) as the major EG oxidation products (Fig. 4a and Supplementary Figs. 23 and 24). These products combined accounted for more than 80% of electrons supplied to syngas production (Fig. 4b) and could be utilized as platform chemicals following separation from the CO₂U chamber. Isotopic labelling experiments with ¹³CO₂ and ¹³EG revealed EG oxidation as the pathway leading to formate and GAD formation without any contribution from the CO₂ reduction pathway (Supplementary Fig. 25). A control experiment with the γ -Al₂O₃|TiO₂ (without CotpyP) showed no CO, and a decreased H₂ production ($\sim 30\%$ of the y-Al₂O₃|TiO₂|CotpyP), confirming the catalytic role of CotpyP in CO₂ and proton reduction reactions (Supplementary Fig. 26). The effect of possible PEI leaching from DAC to the CO₂U chamber during integrated operation (vide infra) was also investigated using 5 wt% PEI in EG as an electron donor. This did not decrease the overall syngas formation rates, but a drop in the CO:H₂ ratio was noted (from 4:1 to 1:3; Supplementary Fig. 27).

Real-world PET waste can also be used as a reductant following KOH-mediated lysis pretreatment (to produce EG) without sacrificing the syngas production activity of the system and is transformed into formate and GAD dimer in the process over a long time (96 h) with syngas formation reaching over 1,500 μ mol per gram of TiO $_2$ at 80% CO selectivity (Fig. 4c, Supplementary Note 4 and Supplementary Fig. 28) 42 .

Investigations towards the response of the fixed-bed flow photoreactor in dilute CO₂ streams revealed a CO production rate roughly proportionate to the CO₂ concentration, whereas the H₂ production remained similar (Fig. 4d and Supplementary Fig. 29). Thus, moving from 100% CO₂ to 50% CO₂ in N₂ (v/v) as the carrier gas, the CO production nearly halved (260 \pm 24 μ mol per gram of TiO₂ versus 156 \pm 16 μ mol per gram of TiO₂ after 12 h). Reasonable activity was observed when air was used as the carrier gas (50% or 20% CO₂), albeit with a notable drop, possibly due to the competing oxygen reduction reaction 43,44. A control experiment with air as both the carrier gas and CO₂ source (400 ppm) produced negligible CO as a CO₂ reduction product, reflecting the need for an upstream CO₂ concentrating unit for effective photoconversion of the atmospheric CO₂. Notably, all experiments with air carrier gas produced a minor background CO (-2 μmol per gram of TiO₂ per hour) due to photoinduced surface impurity oxidation (Supplementary Fig. 30), which was subtracted in all calculations.

DAC and utilization to produce solar fuel

Integrated capture and utilization of CO_2 from air was explored next by combining the capture and utilization bed into a custom-designed tube reactor (Fig. 5a). The DACCU reactor contained an upstream DAC chamber and a downstream CO_2U chamber with an alternate outlet in between to divert the flow around the utilization unit during DAC. Downstream of utilization, an additional chamber was installed for different downstream processing, including the capture of unreacted CO_2 or the further conversion of the generated syngas.

In a standard experiment, the DACCU reactor was loaded with both the SBA-15|PEI (for DAC) and $\gamma\text{-Al}_2O_3|\text{TiO}_2|\text{CotpyP}$ composite (for CO $_2\text{U}$) in their respective compartments and mounted on the axis of a parabolic trough reflector (Supplementary Fig. 31). Humid air (CO $_2$ level 400 ppm) was passed through the capture bed for 12 h (flow rate 90 ml min $^{-1}$) at ambient temperature for DAC in the dark, mimicking night-time operation. During this time, the CO $_2$ level in the outflow mostly remained zero, reflecting effective CO $_2$ removal by the adsorber (Fig. 5b). Following capture, the utilization bed of the CO $_2\text{U}$ unit was moistened with EG, the flow was changed to N $_2$ (1 ml min $^{-1}$) and the solar simulator with concentrator was turned on to mimic daytime operation while holding the moist CO $_2\text{U}$ bed temperature steady at 25 °C. Elevated CO $_2$ levels in the outflow were detected within 10 min owing to effective desorption via photothermal heating (-100 °C; Fig. 5b). GC analysis of the stream showed the initiation of CO and H $_2$ formation by conversion

of the released CO_2 and locally available protons, respectively (Fig. 5b). The CO formation rate followed a similar pattern as the released CO_2 concentration, peaking near 1 h of light-on operation at $8.5 \pm 0.8 \, \mu \text{mol}$ per gram of TiO_2 per hour with high CO_2 levels, and decreasing afterwards with diminished CO_2 availability (Fig. 5b). This result is consistent with the proportional CO_2 production rate dependency on CO_2 concentration observed above (Fig. 4d). Introducing a pure CO_2 feed after 4 h restored the CO_2U catalytic activity of the conversion bed, confirming that the gradual decrease in CO_2 formation is due to limited CO_2 availability with time and not catalyst deactivation (Supplementary Fig. 32). During this time, the H_2 production remained independent of CO_2 levels. These results demonstrate the ability of our developed system to capture, concentrate and convert CO_2 from air into synthesis gas, driven by simulated sunlight and utilizing EG as the electron donor in a moist-bed gas-phase flow reactor setup.

The total CO formation of the system reached around $24 \pm 2 \, \mu mol$ per gram of TiO₂ after 12 h (Fig. 5c). Following conversion, air was reflown through the reactor (90 ml min⁻¹) for a second cycle of capture, and the syngas formation activity of the γ -Al₂O₃|TiO₂|CotpyP composite was partially retained (-50%) during subsequent second cycle conversion (Supplementary Fig. 33). Notably, using air as the carrier gas during utilization decreased CO formation (-80% reduction; Supplementary Fig. 34) while bringing potential complexities to the system involving adsorbent degradation and poisoning of downstream syngas conversion, among others (Supplementary Note 5). As such, N₂ is a preferable carrier gas for the DACCU reactor light-on operation, which also ensures a longer CO₂ adsorbent lifetime and avoids explosive air–fuel gas mixture formation.

The flow system displays high modularity and system flexibility. For example, we could recapture the unreacted CO_2 from the outflow by using a second bed of CO_2 adsorber downstream of the CO_2 U unit. The CO_2 emission during light-on operation from such a modified reactor decreases prominently while keeping the solar syngas production rate unaffected (Fig. 5d). We could also reroute the recaptured CO_2 to the utilization unit by switching the flow direction and irradiation spot, increasing the light-driven CO_2 conversion (Fig. 5e and Supplementary Fig. 35). Single-pass CO_2 conversion can also be improved in theory by using a larger utilization unit, improved light management and optimized reactor design 46,47. The produced syngas can also be theoretically converted into liquid fuels in additional downstream syngas conversion units or used in carbonylative hydrogenation reactions (Supplementary Fig. 36), utilizing the benefits of a flow system for easy process integration 48.

Discussion

We demonstrate an integrated DACCU flow reactor that captures, concentrates and converts CO_2 from air into renewable synthesis gas using simulated sunlight. We envision running the process diurnally where CO_2 can be captured upstream during night-time operation (light off) and subsequently released and converted downstream during daytime operation (light on) using incident sunlight. Our approach offers a promising way for direct on-site utilization of CO_2 at DAC plants using sunlight without requiring high temperature or pressure, rather than transporting and storing the CO_2 .

At the same time, the strategy of DAC and the release of CO_2 in concentrated form before conversion provide a promising solution to the challenges of low CO_2 concentration (0.04%) and high O_2 presence (21%) in solar CO_2 reduction chemistry from air. O_2 reduction is a favourable reaction that often dominates CO_2 reduction when present in the stream $^{49-51}$. By introducing a temporal separation between CO_2 capture and reduction and providing means to concentrate CO_2 and remove O_2 upstream, our approach provides a solution to both CO_2 -scarcity and O_2 -poisoning challenges.

The CO_2 adsorbent we use in this study has high DAC efficiency and capacity and releases CO_2 under solar photothermal heating. Our process is not limited to the SiO_3 [PEI composite for DAC and is compatible

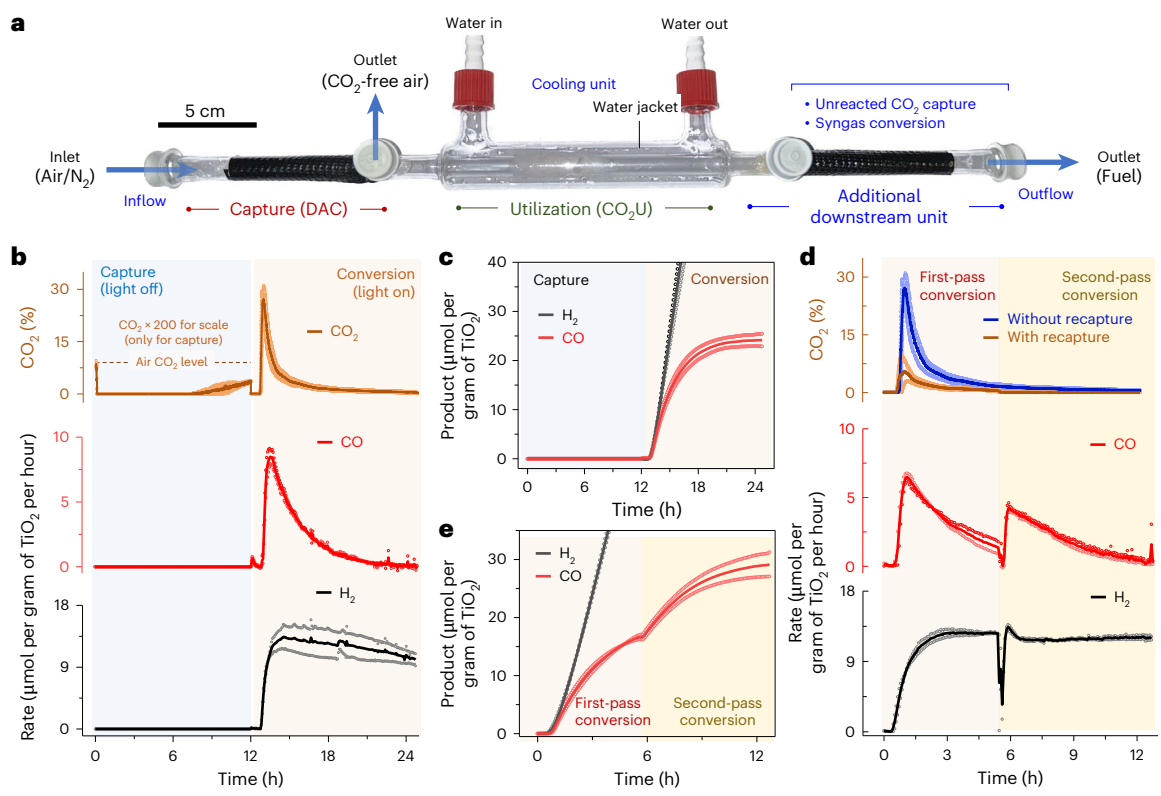


Fig. 5 | DACCU to produce solar syngas. a, The designed reactor for in-flow DAC and CO_2U . b, CO_2 levels and photocatalytic CO and H_2 formation rates in the outflow during DACCU. The CO_2 values during capture $(0-12\,h)$ are multiplied by a factor of 200 for ease of visualization. DAC was performed during light-off operation at room temperature under airflow $(90\ ml\ min^{-1})$ and the CO_2U is carried out during light-on operation under 3-sun illumination at 25 °C under N_2 flow $(1\ ml\ min^{-1})$. c, Cumulative H_2 and CO yield over time during DACCU.

 $oldsymbol{d}$, Recapture and rerouting of unreacted CO $_2$ for increased conversion and low carbon emission. The additional downstream unit was loaded with fresh adsorbents for unreacted CO $_2$ capture and rerouting during conversion. $oldsymbol{e}$, Cumulative H $_2$ and CO formation over time during first- and second-pass conversion during operation under simulated solar irradiation. Data are presented as the average of two independent runs, and the individual data points are shown in hollow circles.

with other CO_2 adsorbents that release CO_2 upon heating around 80– $100\,^{\circ}$ C, including zeolites 52,53 , metal–organic frameworks 54,55 and covalent–organic frameworks 56,57 , and can be tuned to accommodate contemporary progresses in CO_2 sorbent developments. The CO_2 U unit is based on a molecular–semiconductor hybrid material, which is a promising approach in gas-phase CO_2 conversion. The moist-bed gas-phase flow CO_2 U unit enables easy process integration with the upstream gas-phase DAC unit while overcoming the solution-phase limitations of low gaseous CO_2 availability 26 .

Future focus will be on devising methods for supplying long-term continuous reactant feed to the reactor and product separation off the reactor (Supplementary Note 6). The development of IR photothermal heat-resistant $\rm CO_2$ conversion catalysts that can utilize the full UV–vis solar spectrum would unlock the complete benefits of the solar reflector by utilizing the UV–vis light for photoconversion and the IR photothermal heat to expedite the conversion process (Supplementary Note 7). These future developments would be needed to enable the practical implementation of this DACCU process, powered directly by the energy from the Sun.

Methods

Materials

Silica nanopowder (nSiO₂, 5–20 nm, ≥99%, Sigma), mesoporous silica SBA-15 (<150 µm particle size, pore size 8 nm, Sigma), gamma alumina nanoparticles (γ -Al₂O₃, <50 nm, ≥99%, Sigma), mesoporous alumina (mAl₂O₃, pore type MSU-X, average pore size 3.8 nm, Sigma), cerium (IV) oxide nanopowder (nCeO₂, <25 nm, Sigma), titania nanopowder (TiO₂, particle size <21 nm, Sigma), branched PEI (weight-average molecular

weight 25,000 g per mole, Sigma), methanol (\geq 99%, Sigma), ethanol (\geq 99%, Sigma), EG (\geq 99%, Sigma), glycerol (\geq 99%, Sigma), tetrahydrofuran (THF, Fisher Scientific, HPLC grade, 98%) and potassium hydroxide (Fischer Scientific, Analytical reagent grade) were used as received. CO₂ (CP grade, British Oxygen Company (BOC)), N₂ (99.99%, BOC), artificial air (400 ppm CO₂ in 21% O₂ and balance N₂, BOC), carbon-¹³C dioxide (13 CO₂, 99.0 atom% 13 C, Sigma-Aldrich), EG-d₆ (98% D, Sigma) and 13 C-EG (95.0 atom% 13 C, Sigma-Aldrich) were used without further purification unless otherwise stated. Molecular complex [Co(2,2':6',2''-terpyridine-4'-phosphonic acid)₂](BF₄)₂ (denoted as CotpyP) was prepared following a reported procedure 36 . For PET waste, plastic bottles from Sainsbury's Cola (internal volume 2 I, unrecycled PET) were used after removing the label sticker, rinsing with deionized water and drying at 110 °C for 1 h.

Material and product characterization

The gas products were analysed with a Shimadzu GC-2010 Plus gas chromatogram with ultrapure Helium (CP Grade) as the carrier gas. The chromatographic separations for the oxidation products were conducted using a Waters HPLC system equipped with a Phenomenex Rezex 8% H $^{+}$ column at a column temperature of 60 °C. The samples were analysed in the isocratic flow mode (flow rate: 0.5 ml min $^{-1}$, 0.0025 Maqueous H $_{2}$ SO $_{4}$) using a Waters breeze HPLC system equipped with refractive index (RIS-2414) and diode array UV-vis (λ = 254 nm) detectors. For the 13 C-isotope labelling experiments, 13 CO was detected using IR spectroscopy (Thermo Scientific Nicolet iS50 IR spectrometer) in the gas-phase transmission mode. The headspace from the cell was transferred to an air-tight evacuated IR cell (path length 10 cm, equipped with KBr windows) after the experiment for the detection of

 ^{13}CO (data resolution 0.125, data spacing 0.060 cm $^{-1}$). Attenuated total reflectance Fourier transform IR spectra were recorded in a Thermo Scientific Nicolet iS50 IR spectrometer in reflectance mode. UV–vis diffused reflectance spectra were recorded using a Bruker Cary 60 UV–vis spectrophotometer. The powder X-ray diffraction measurements of the samples were performed using a Panalytical X'Pert Pro (Cu Kα radiation) diffractometer with a 2 θ (θ = angle of incidence) range from 10° to 80° at a scan rate of 1° min $^{-1}$.

The SEM images and EDS maps were acquired using a TESCAN MIRA3 FEG-SEM instrument (operated at 5 kV) equipped with an Oxford Instruments Aztec Energy X-maxN 80 EDS system. The transmission electron microscopy (TEM), bright-field STEM, high-angle annular dark-field (HAADF) STEM images and EDS maps were acquired using a Thermo Scientific Talos F200X G2 transmission electron microscope (operating voltage 200 kV). Transmission electron microscopy images were acquired using a Thermo Scientific Ceta complementary metal oxide semiconductor camera. STEM images were collected using a Thermo Scientific bright-field detector and Fischione HAADF detector at a camera length of 98 mm and EDS maps using a Super-X detector system. Samples were prepared by drop-casting a dilute composite solution on holey-carbon-coated Cu grids or lacey-carbon-coated Ni grids followed by evaporation of the solvent.

The ICP-OES measurements were performed on a Thermo Scientific iCAP 7400 ICP-OES DUO spectrometer at the Microanalysis Service, Yusuf Hamied Department of Chemistry, University of Cambridge. CO₂ was detected using a Gas Sensing Solutions CozIR-LP (0-2,000 ppm) sensor during air capture and using a SprintIR-6S CO₂ sensor (0–100%) during desorption. Nitrogen physisorption isotherms were measured using Micromeritics 3Flex Adsorption Analyzer. All the materials were degassed for a few hours under vacuum before measurement. Nitrogen adsorption and desorption isotherms were measured at 77 K. The specific surface area was calculated by the multipoint BET method using the adsorption branch of the physisorption isotherm. The total pore volume was determined at relative pressure (P/Po) close to 1. TGA measurements were taken in a Mettler Toledo Thermogravimetric Analyser under an airflow of 100 ml min⁻¹ in a temperature range from 25 °C to 800 °C with a heating rate of 5 °C min⁻¹ (temperature holding time at 800 °C = 10 min). The initial weight loss observed below 150 °C was attributed to the loss of adsorbed moisture and CO₂. The weight loss from 150 °C to 800 °C was counted towards the organic content. The thermal images were taken using a FLIR ONE Gen 3 thermal camera. Mass spectrometry was recorded using a Hiden Analytical HPR-20 benchtop gas analysis system to a HAL 101 RC electron impact quadrupole mass spectrometer with a Faraday detector. The nuclear magnetic resonance measurements were performed in a Brooker Biospin instrument at room temperature (298 K). The XPS measurements were performed at the Maxwell Centre, University of Cambridge, with a near-ambient-pressure XPS system using a SPECS XR 50 MF X-ray source, μ-FOCUS 600 X-ray monochromator and a differentially pumped PHOIBOS 150 1D-DLD near-ambient-pressure analyser. The peak positions were calibrated with respect to the C1s binding energy at 286 eV, and Casa-XPS software was used for the curve fitting and deconvolution.

$Preparation \, of \, CO_2 \, capture \, composite$

Three grams of PEI was dissolved in 20 ml methanol and was subsequently added dropwise to a suspension of 3 g SBA-15 silica on 200 ml methanol under vigorous stirring. The resulting solution was stirred overnight. The solvent was subsequently removed under reduced pressure (85 mbar) at 40 °C and dried overnight under high vacuum to afford a solid powder composite (SBA-15|PEI), which was analysed by SEM, EDS, BET and TGA and used for DAC 58 .

Preparation of CO₂ conversion hybrid composite

Here, 0.5 mg of CotpyP was dissolved in 5 ml methanol and was subsequently added dropwise to a suspension of 50 mg TiO₂ (P25) on 10 ml

methanol under stirring. The resulting TiO₂|CotpyP hybrid suspension was stirred for 2 h (ref. 35). Subsequently, the suspension was added dropwise to a suspension of 1 g of support (nSiO₂/SBA-15/ γ -Al₂O₃/mAl₂O₃/nCeO₂) in 100 ml methanol. The resulting solution was stirred overnight. The solvent was subsequently removed under reduced pressure (85 mbar) at 40 °C and dried overnight under high vacuum to afford a solid powder composite that was examined by SEM, TEM, EDS, BET, XRD, IR and UV–vis analyses and was directly used for CO₂ conversion studies.

Design and construction of the parabolic trough reflector

The parabolic trough reflector was constructed from two three-dimensional (3D)-printed parabolic endpieces combined with highly reflective (90%+ solar reflectance) Alanod MIRO-SUN 20901L aluminium sheeting to create a parabolic trough solar concentrator. The parabolic endpieces were designed using Autodesk Inventor, with the curve of the parabola being defined in Cartesian coordinates by the equation $y = (x^2)/32$ with the focus and point of light concentration at (x, y) = (0, 8) (Supplementary Fig. 5b). The reactor was built to be 32 cm wide (owing to the size of available simulated solar light sources), making the focus of the parabolic trough concentrator at a height equal to the height of the parabolic endpieces, with the focus line running down the centre of the symmetrical parabolic trough. Three 1.0-cm-diameter holes were designed in each endpiece, so the two sides of the reactor could be connected using 1.0-cm-diameter Delrin rods, which were press-fit to connect the two reactor endpieces. A piece of Alanod sheeting was then attached using high-strength double-sided fastening tape. Two sample holder crossbeams (Supplementary Fig. 5) were also 3D printed to hold a borosilicate glass reaction tube with an 11 mm outer diameter at the focus of the parabolic trough concentrator. When constructed, the reactor had a length of 25 cm, including the two endpieces. All 3D-printed reactor parts were printed using Ultimaker Tough polylactic acid material using an Ultimaker S5 printer.

Direct air CO₂ capture and solar photothermal desorption

The adsorbent was treated under reduced pressure (<1 mbar) at 50 °C for an hour before DAC. Subsequently, in a tubular glass reactor, 600 mg of solid CO $_2$ adsorbent was loaded and fixed inside the reactor using glass wool plugins. The tube was then closed, and humid air (relative humidity -60%) was passed through the adsorber bed at 90 ml min $^{-1}$ flow rate using a mass flow controller (MFC; Brooks GF040) under ambient temperature. The CO $_2$ levels in the outlet stream were recorded using a CoZIR CO $_2$ sensor from Gas Sensing Solutions (0–2,000 ppm). The sensor was calibrated before each experiment using nitrogen (0 ppm) and air (400 ppm). The time profile of CO $_2$ loadings onto the adsorbent was calculated by integrating the removed CO $_2$ concentration with time multiplied by flow rate.

For the desorption studies, a direct air CO_2 capture experiment was first performed for around 20 h. The adsorber bed was then wrapped with an IR-absorbing photothermal material on top of the glass reactor. For this purpose, a black-coloured Gaffa tape (Faithfull Quality Tools) was used. The tube was then placed at the focal axis of the parabolic trough solar reflector and placed inside the solar simulator. Air was subsequently flown through the adsorber bed as carrier gas $(0.5-3 \text{ ml min}^{-1})$, and the solar simulator light (Newport Oriel, AM 1.5G, 100 mW cm^{-2}) was turned on (t=0), wherein t stands for time). The CO_2 levels of the output stream were detected using a Gas Sensing Solutions Sprint-IR CO_2 sensor (0-100%), which was calibrated before each experiment using N_2 (0%) and pure CO_2 (100%).

CO₂ photoreduction procedure in batch

A glass photo vial was loaded with 100 mg of solid CO_2 reduction material ($nSiO_2|TiO_2|CotpyP$) which was subsequently moistened with 0.15 ml of electron donors (water, methanol, ethanol, EG or glycerol). The headspace of the vial was then purged with humid CO_2 (containing

 $2\%\,CH_4$ as internal standard), and the vial was irradiated with simulated solar light (Newport Oriel, 100 mW cm $^{-2}$, AM1.5G) for 20 h, keeping the temperature at 25 °C. Afterwards, an aliquot of the headspace gas was analysed by GC via manual injection to determine the H_2 and CO yield. The residual solid was then suspended in 1 ml water, and the resulting mixture was filtered. The filtrate was analysed by HPLC for oxidation product determination.

Moist-bed gas-phase CO₂ photoreduction procedure in flow

In a tubular glass reactor (length 28 cm, inner diameter 0.6 cm), 250 mg of CO₂ conversion composite (support|TiO₂|CotpyP) was loaded. Subsequently, the composite was manually moistened with EG by adding 0.50 ml EG dropwise using a pipette. The tube was subsequently sealed with septa at both ends and placed into the focal axis of the parabolic trough reflector. Humidified carrier gas (nitrogen, CO2 and air) was subsequently flown through the tube at a constant flow rate (1-5 ml min⁻¹) using an MFC (Brooks GF040) while keeping the reactor inside a simulated solar simulator (lamp off). The outlet of the reactor was connected to an online GC through a 1 ml loop that injected approximately every 4.25 min into the GC. The flow rate at the GC outlet was verified before the experiment with an Alicat gas flow meter to ensure no gas leakage. The initial 45 min of the experiments were run in the dark to obtain a stable GC baseline, after which the solar simulator lamp (Newport Oriel, AM 1.5G, 100 mW cm⁻²) was turned on for 12 h. The momentary rates of CO and H_2 evolution (\dot{n}_{gas}) from individual injections were determined from the GC responses by subtracting the baseline under dark conditions and using a previously described procedure with the same setup⁵⁹ using

$$\dot{n}_{\rm gas} = \frac{p \times \dot{V} \times \frac{\rm area\ GC}{f_i}}{R \times T},\tag{1}$$

where p is the pressure in the flow reactor (ambient pressure, 101,325 bar), \dot{V} is the flow rate, R is the universal gas constant, T is the temperature before injection (298 K) and f_i is the response factor of each gas determined by a calibration procedure. The GC calibration was performed with a known standard for H_2 , CO and CH_4 (4,000 ppm H_2 /4,000 ppm CO/1,000 ppm CH_4 in balance gas CO_2 , BOC) by diluting the mixture with pure CO_2 . The CO selectivity values were obtained by dividing momentary CO evolution rates by total combined momentary rates of CO and CO and CO evolution. The amount of evolved product with time was calculated by integrating the product evolution rates with time. The CO and the CO with respect to the molecular catalyst were calculated using

$$TON_{product} = \frac{moles \text{ of specific product formed}}{moles \text{ of molecular catalyst present}}$$
 (2)

$$TOF_{product} = \frac{TON_{product}}{time(h)}.$$
 (3)

For the reactions under 1 sun, the reflector surface of the trough reflector was covered with a non-reflective material (white paper). For reactions under 3 suns, the paper cover was removed to ensure solar concentration. For the reactions at 25 °C, water was circulated through a water jacket on the reactor using a chiller to ensure a steady temperature. For HPLC analysis of the oxidation products, the glass wool plugs were carefully removed from the reactor after the reaction. The composite was then recovered in a vial and sonicated after adding 2 ml of deionized water. The resulting mixture was then filtered using a syringe filter, and the liquid was analysed by HPLC.

For the isotope labelling study with $^{13}CO_2$, the experiment was carried out in batch. The tube was filled with $^{13}CO_2$ and sealed instead of continually passing $^{13}CO_2$. The sealed tube was then irradiated under 1 sun for 20 h, after which the gas inside was analysed with IR

spectroscopy in transmission mode, which showed the formation of 13 C-labelled CO. For dilute concentration CO₂ reactions (20–50% v/v), CO₂ was mixed upstream with N₂ or air using MFCs to the desired concentrations with a total flow rate of either 2 ml min⁻¹ (50% CO₂) or 5 ml min⁻¹ (20% CO₂).

For the reactions with real-world PET waste as a reductant, PET plastic from a plastic bottle was shredded. Following that, 100 g of shredded PET was suspended in a solvent mixture of methanol and THF (400 ml and 100 ml, respectively). Subsequently, 56 g of KOH was added, and the resultant mixture was stirred at 60 °C for 24 h (Supplementary Note 4). Afterwards, the solution was filtered to remove the precipitated dipotassium terephthalate, and the THF and MeOH were removed from the filtrate under reduced pressure. EG was extracted from the remaining mixture through vacuum distillation (yield 19.4 g, 60%), which was then directly used in the DACCU reactor. For the PET breakdown in EG solvent, 5 g of PET was suspended in 25 ml of EG, followed by the addition of 2.8 g KOH. The resultant mixture was stirred at 150 °C for 4 h. Subsequently, the solution was left undisturbed for 24 h (to precipitate the dipotassium terephthalate). The EG was then decanted from the mixture, containing both solvent EG and PET-derived EG, and was used in the reaction. The breakdown of PET plastic was verified in this case by characterizing and quantifying the dipotassium terephthalate product by ¹H and ¹³C nuclear magnetic resonance spectroscopy (5.1 g, 81%).

DAC of CO₂ and solar-driven conversion

The modified tubular reactor, as shown in Fig. 5a, was used for integrated capture and conversion. First, the DACCU tube was loaded with 600 mg of CO₂ adsorbent in the capture compartment and 250 mg of CO₂ conversion composite in the downstream conversion chamber. Air was then flown through the capture bed for 12 h (flow rate 90 ml min⁻¹), and an alternate outlet was used to bypass the flow around the conversion chamber. The CO₂ concentration in the outflow during capture was monitored using a CO₂ sensor, and the H₂ and CO levels were not monitored (assumed zero). Following the capture, the CO₂ conversion bed was moistened with 0.50 ml EG, and the reactor was then sealed and placed inside a solar simulator (lamp off). Humid nitrogen or air was then passed through the capture and conversion unit as carrier gas (1 ml min⁻¹), and the CO₂, CO and H₂ levels of the outlet stream were measured using a CO₂ sensor (CO₂) or GC (CO and H₂). The first 45 min of conversion was done without light to obtain a stable baseline, after which the solar simulator lamp was turned on for 12 h. The temperature of the conversion unit was kept at 25 °C throughout the experiment using a chiller. The CO responses were corrected by subtracting a background response from a blank reaction in pure N₂ or air (Supplementary Fig. 30).

For the reaction with multiple capture and conversion cycles, the first cycle of capture and conversion was carried out as described. Subsequently, air was flown again through the $\rm CO_2$ adsorbent, and the outlet gas stream was bypassed around the conversion unit using an alternate outlet and a placed septum before the conversion unit. After 12 h of capture, the septum was removed, and the reloaded $\rm CO_2$ adsorbent was used for subsequent conversion, following similar procedures as in the first cycle.

For the recapture of unreacted CO_2 followed by double-pass conversion, CO_2 capture was first carried out using the procedure previously stated in the capture chamber. Subsequently, the conversion chamber was loaded with the CO_2 conversion composite, moistened with EG, and another layer of fresh CO_2 adsorbent (700 mg) was loaded in the downstream additional chamber. The resulting reactor was then placed in the focal axis of the parabolic trough reflector. The reactor was then placed inside the solar simulator, humid N_2 was flown through it as carrier gas, and the output CO_2 , CO and CO_2 sensor and CO_2 conversion unit while the turned on, irradiating only the capture and conversion unit while

keeping the downstream unreacted CO_2 capture unit in the dark. After about 6 h, as the CO_2 and CO levels in the outlet almost subsided, the inlet and outlet of the reactor were switched, and concentrated light was selectively shone in the conversion unit and the captured unreacted CO_2 unit (Supplementary Fig. 35). The experiment was continued for another 6 h after which the light was turned off.

For the reaction introducing pure CO_2 after 4 h to check for any possible catalyst deactivation (Supplementary Fig. 32), a standard direct air carbon capture and solar-driven conversion reaction was set up as described above. After 4.25 h of solar irradiation during conversion, the carrier gas was switched from humid nitrogen (1 ml min⁻¹) to humid CO_2 (5 ml min⁻¹). The conversion was continued for an additional 3 h as the generated CO and H_2 rates were measured using GC.

Reporting summary

Further information on research design is available in the Nature Portfolio Reporting Summary linked to this article.

Data availability

The raw data supporting the findings of this study are available via the Apollo – University of Cambridge data repository at https://doi. org/10.17863/CAM.114082.2 (ref. 60). Source data are provided with this paper.

References

- Sanz-Pérez, E. S., Murdock, C. R., Didas, S. A. & Jones, C. W. Direct capture of CO₂ from ambient air. Chem. Rev. 116, 11840–11876 (2016).
- McQueen, N. et al. A review of direct air capture (DAC): scaling up commercial technologies and innovating for the future. Prog. Energy 3, 032001 (2021).
- Erans, M. et al. Direct air capture: process technology, techno-economic and socio-political challenges. Energy Environ. Sci. 15, 1360–1405 (2022).
- Chauvy, R. & Dubois, L. Life cycle and techno-economic assessments of direct air capture processes: an integrated review. *Int. J. Energy Res.* 46, 10320–10344 (2022).
- 5. Bui, M. et al. Carbon capture and storage (CCS): the way forward. Energy Environ. Sci. 11, 1062–1176 (2018).
- Martin-Roberts, E. et al. Carbon capture and storage at the end of a lost decade. One Earth 4, 1569–1584 (2021).
- Yousaf, M. et al. Carbon dioxide utilization: a critical review from multiscale perspective. Energy Sci. Eng. 10, 4890–4923 (2022).
- vom Berg, C. & Carus, M. 2023: Making a Case for Carbon Capture and Utilisation (CCU)—It Is Much More Than Just a Carbon Removal Technology (Renewable Carbon Initiative, 2023).
- Victoria, M. et al. Solar photovoltaics is ready to power a sustainable future. *Joule* 5, 1041–1056 (2021).
- Maka, A. O. M. & Alabid, J. M. Solar energy technology and its roles in sustainable development. *Clean Energy* 6, 476–483 (2022).
- Schäppi, R. et al. Drop-in fuels from sunlight and air. Nature 601, 63–68 (2022).
- 12. Lin, H., Luo, S., Zhang, H. & Ye, J. Toward solar-driven carbon recycling. *Joule* **6**, 294–314 (2022).
- Gong, E. et al. Solar fuels: research and development strategies to accelerate photocatalytic CO₂ conversion into hydrocarbon fuels. Energy Environ. Sci. 15, 880–937 (2022).
- Bagger, A., Christensen, O., Ivaništšev, V. & Rossmeisl, J. Catalytic CO₂/CO reduction: gas, aqueous, and aprotic phases. ACS Catal. 12, 2561–2568 (2022).
- Schreck, M. & Niederberger, M. Photocatalytic gas phase reactions. Chem. Mater. 31, 597–618 (2019).

- Matter, F. & Niederberger, M. The importance of the macroscopic geometry in gas-phase photocatalysis. Adv. Sci. 9, 2105363 (2022).
- Moustakas, N. G. et al. A high-purity gas-solid photoreactor for reliable and reproducible photocatalytic CO₂ reduction measurements. *HardwareX* 15, e00448 (2023).
- 18. Dilla, M., Schlögl, R. & Strunk, J. Photocatalytic CO_2 reduction under continuous flow high-purity conditions: quantitative evaluation of CH_4 formation in the steady-state. *ChemCatChem* **9**, 696–704 (2017).
- Moruzzi, F. et al. Solution-processable polymers of intrinsic microporosity for gas-phase carbon dioxide photoreduction. *Nat. Commun.* 14, 3443 (2023).
- 20. Ali, S. et al. Gas phase photocatalytic CO₂ reduction, "A brief overview for benchmarking". *Catalysts* **9**, 727 (2019).
- Sorcar, S., Yoriya, S., Lee, H., Grimes, C. A. & Feng, S. P. A review of recent progress in gas phase CO₂ reduction and suggestions on future advancement. *Mater. Today Chem.* 16, 100264 (2020).
- Direct Air Capture 2022 (IEA, 2022); https://www.iea.org/reports/ direct-air-capture-2022
- 23. Coy, E., latsunskyi, I. & Bechelany, M. Perspectives and current trends on hybrid nanocomposite materials for photocatalytic applications. *Sol. RRL* **7**, 2201069 (2023).
- Shang, B. et al. Monolayer molecular functionalization enabled by acid-base interaction for high-performance photochemical CO₂ reduction. ACS Energy Lett. 7, 2265–2272 (2022).
- 25. Goeppert, A. et al. Carbon dioxide capture from the air using a polyamine based regenerable solid adsorbent. *J. Am. Chem. Soc.* **133**, 20164–20167 (2011).
- Goeppert, A. et al. Easily regenerable solid adsorbents based on polyamines for carbon dioxide capture from the air. ChemSusChem 7, 1386–1397 (2014).
- Ozkan, M., Nayak, S. P., Ruiz, A. D. & Jiang, W. Current status and pillars of direct air capture technologies. *iScience* 25, 103990 (2022).
- Wiegner, J. F., Grimm, A., Weimann, L. & Gazzani, M. Optimal design and operation of solid sorbent direct air capture processes at varying ambient conditions. *Ind. Eng. Chem. Res.* 61, 12649– 12667 (2022).
- Bhattacharjee, S. et al. Photoelectrochemical CO₂-to-fuel conversion with simultaneous plastic reforming. *Nat. Synth.* 2, 182–192 (2023).
- 30. Kar, S. et al. Integrated capture and solar-driven utilization of CO₂ from flue gas and air. *Joule* **7**, 1496–1514 (2023).
- 31. Moustakas, N. G., Lorenz, F., Dilla, M., Peppel, T. & Strunk, J. Pivotal role of holes in photocatalytic CO₂ reduction on TiO₂. *Chem. Eur. J.* **27**, 17213–17219 (2021).
- 32. Tan, H. W., Abdul Aziz, A. R. & Aroua, M. K. Glycerol production and its applications as a raw material: a review. *Renew. Sustain. Energy Rev.* **27**, 118–127 (2013).
- Bhattacharjee, S. et al. Reforming of soluble biomass and plastic derived waste using a bias-free Cu₃₀Pd₇₀|perovskite|Pt photoelectrochemical device. Adv. Funct. Mater. 32, 2109313 (2022).
- 34. Zhu, J. Y. & Pan, X. Efficient sugar production from plant biomass: current status, challenges, and future directions. *Renew. Sustain. Energy Rev.* **164**, 112583 (2022).
- Lam, E. & Reisner, E. A TiO₂-Co(terpyridine)₂ photocatalyst for the selective oxidation of cellulose to formate coupled to the reduction of CO₂ to syngas. *Angew. Chem. Int. Ed.* 60, 23306– 23312 (2021).
- Leung, J. J. et al. Solar-driven reduction of aqueous CO₂ with a cobalt bis(terpyridine)-based photocathode. *Nat. Catal.* 2, 354–365 (2019).

- Augugliaro, V. et al. Overview on oxidation mechanisms of organic compounds by TiO₂ in heterogeneous photocatalysis. J. Photochem. Photobiol. C 13, 224–245 (2012).
- Najafishirtari, S. et al. A perspective on heterogeneous catalysts for the selective oxidation of alcohols. Chem. Eur. J. 27, 16809–16833 (2021).
- 39. Wagner, A., Sahm, C. D. & Reisner, E. Towards molecular understanding of local chemical environment effects in electroand photocatalytic CO₂ reduction. *Nat. Catal.* **3**, 775–786 (2020).
- Busca, G. Catalytic materials based on silica and alumina: structural features and generation of surface acidity. *Prog. Mater Sci.* 104, 215–249 (2019).
- Ostadi, M., Rytter, E. & Hillestad, M. Boosting carbon efficiency of the biomass to liquid process with hydrogen from power: the effect of H₂/CO ratio to the Fischer-Tropsch reactors on the production and power consumption. *Biomass Bioenergy* 127, 105282 (2019).
- 42. Bhattacharjee, S., Linley, S. & Reisner, E. Solar reforming as an emerging technology for circular chemical industries. *Nat. Rev. Chem.* **8**, 87–105 (2024).
- Kim, J.-H., Ishihara, A., Mitsushima, S., Kamiya, N. & Ota, K.-I. Catalytic activity of titanium oxide for oxygen reduction reaction as a non -platinum catalyst for PEFC. *Electrochim. Acta* 52, 2492–2497 (2007).
- 44. Song, C. et al. in *Studies in Surface Science and Catalysis* Vol. 153 (eds Park, S.-E. et al.) 315–322 (Elsevier, 2004).
- Wang, Q., Pornrungroj, C., Linley, S. & Reisner, E. Strategies to improve light utilization in solar fuel synthesis. *Nat. Energy* 7, 13–24 (2022).
- Andrei, V., Wang, Q., Uekert, T., Bhattacharjee, S. & Reisner, E. Solar panel technologies for light-to-chemical conversion. Acc. Chem. Res. 55, 3376–3386 (2022).
- Nguyen, V.-H. & Wu, J. C. S. Recent developments in the design of photoreactors for solar energy conversion from water splitting and CO₂ reduction. Appl. Catal. A 550, 122–141 (2018).
- 48. Chuang, S. S. C. in *Handbook of Climate Change Mitigation* (eds Chen, W.-Y. et al.) 1605–1621 (Springer, 2012).
- Xu, Y. et al. Oxygen-tolerant electroproduction of C₂ products from simulated flue gas. Energy Environ. Sci. 13, 554–561 (2020).
- 50. Lu, X. et al. A bio-inspired O₂-tolerant catalytic CO₂ reduction electrode. Sci. Bull. **64**, 1890–1895 (2019).
- Cobb, S. J., Dharani, A. M., Oliveira, A. R., Pereira, I. A. C. & Reisner, E. Carboxysome-inspired electrocatalysis using enzymes for the reduction of CO₂ at low concentrations. *Angew. Chem. Int. Ed.* 62, e202218782 (2023).
- 52. Fu, D. & Davis, M. E. Toward the feasible direct air capture of carbon dioxide with molecular sieves by water management. *Cell Rep. Phys. Sci.* **4**, 101389 (2023).
- Boer, D. G., Langerak, J. & Pescarmona, P. P. Zeolites as selective adsorbents for CO₂ separation. ACS Appl. Energy Mater. 6, 2634–2656 (2023).
- Trickett, C. A. et al. The chemistry of metal-organic frameworks for CO₂ capture, regeneration and conversion. *Nat. Rev. Mater.* 2, 17045 (2017).
- 55. Bose, S. et al. Challenges and opportunities: metal-organic frameworks for direct air capture. *Adv. Funct. Mater.* **34**, 2307478 (2023).
- 56. Lyu, H., Li, H., Hanikel, N., Wang, K. & Yaghi, O. M. Covalent organic frameworks for carbon dioxide capture from air. *J. Am. Chem.* Soc. **144**, 12989–12995 (2022).
- 57. Zhou, Z. et al. Carbon dioxide capture from open air using covalent organic frameworks. *Nature* **635**, 96–101 (2024).
- Goeppert, A., Meth, S., Prakash, G. K. S. & Olah, G. A. Nanostructured silica as a support for regenerable highcapacity organoamine-based CO₂ sorbents. *Energy Environ. Sci* 3, 1949–1960 (2010).

- Sahm, C. D., Ucoski, G. M., Roy, S. & Reisner, E. Automated and continuous-flow platform to analyze semiconductor-metal complex hybrid systems for photocatalytic CO₂ reduction. ACS Catal. 11, 11266–11277 (2021).
- Kar, S. et al. Dataset for "Direct air capture of CO₂ for solar fuels production in flow". Apollo – Univ. Cambridge Repository https://doi.org/10.17863/CAM.114082.2 (2024).

Acknowledgements

This work was supported by the Engineering and Physical Sciences Research Council (grant ref.: EP/X023370/1 to S. Kar, EP/X024822/1 to B.B.S., EP/Y024273/1 to S. Karak and EP/S022953/1 with NanoFutures Leadership Award to S.B.), the European Research Council (ERC) with a proof-of-concept grant (SolReGen: to E.R.), UK Research and Innovation (UKRI, ERC Advanced Grant, EP/X030563/1 to E.R., domino4chem), UKRI Cambridge Circular Plastics Centre (CirPlas, EP/S025308/1 to E.R.), UK's Department of Science, Innovation and Technology and the Royal Academy of Engineering Chair in Emerging Technologies programme (CIET-2324-83 to E.R.), the Swiss National Science Foundation (Early Postdoc Fellowship: P2EZP2-191791 to E.L.), the Petronas Education Sponsorship Programme for Postgraduate Studies (to A.B.M.A.), the Cambridge Trust (HRH The Prince of Wales Commonwealth Scholarship to S.B.) and the Hermann and Marianne Straniak Stiftung (to E.R.). We acknowledge the EPSRC Underpinning multiuser equipment call (EP/P030467/1) for funding the TEM. We also acknowledge S. Lee (Department of Chemistry, University of Cambridge) for useful feedback on the manuscript.

Author contributions

Conceptualization—S. Kar and E.R.; investigation—S. Kar, D.K., A.B.M.A., B.B.S., M.S., S. Karak and H.F.G.; methodology—S. Kar and E.L.; project administration—S. Kar and E.R.; supervision—S. Kar and E.R.; visualization—S. Kar, B.B.S., S.B. and S. Karak; writing (original draft)—S. Kar and E.R.; writing (review and editing)—S. Kar, D.K., A.B.M.A., B.B.S., M.S., E.L., S.B., S. Karak, H.F.G. and E.R.

Competing interests

A patent application covering integrated direct air capture and utilization into solar fuels has been submitted on behalf of the University of Cambridge via its technology transfer office, Cambridge Enterprise with co-inventors S. Kar and E.R. (application no. GB2408950.0). The other authors declare no competing interests.

Additional information

Supplementary information The online version contains supplementary material available at https://doi.org/10.1038/s41560-025-01714-y.

Correspondence and requests for materials should be addressed to Erwin Reisner.

Peer review information *Nature Energy* thanks Matthew Potter and the other, anonymous, reviewer(s) for their contribution to the peer review of this work.

Reprints and permissions information is available at www.nature.com/reprints.

Publisher's note Springer Nature remains neutral with regard to jurisdictional claims in published maps and institutional affiliations.

Open Access This article is licensed under a Creative Commons Attribution 4.0 International License, which permits use, sharing, adaptation, distribution and reproduction in any medium or format, as long as you give appropriate credit to the original author(s) and the source, provide a link to the Creative Commons licence, and indicate if changes were made. The images or other third party material in this article are included in the article's Creative Commons licence, unless indicated otherwise in a credit line to the material. If material is not included in the article's Creative Commons licence and your intended

use is not permitted by statutory regulation or exceeds the permitted use, you will need to obtain permission directly from the copyright holder. To view a copy of this licence, visit http://creativecommons.org/licenses/by/4.0/.

© The Author(s) 2025